Neurobiology of Disease 150 (2021) 105253

Contents lists available at ScienceDirect

Neurobiology of Disease

journal homepage: www.elsevier.com/locate/ynbdi

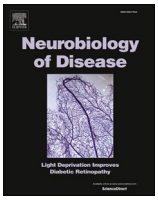

FMRP regulates the subcellular distribution of cortical dendritic spine density in a non-cell-autonomous manner

Katherine M. Bland [a,1], Adam Aharon [b,1], Eden L. Widener [a], M. Irene Song [a], Zachary O. Casey [a], Yi Zuo [b,*], George S. Vidal [a,*]

[a] Department of Biology, James Madison University, Harrisonburg, VA 22801, United States
[b] Department of Molecular, Cell and Developmental Biology, University of California Santa Cruz, Santa Cruz, CA 95064, United States

ARTICLE INFO

Keywords:
Fragile X Syndrome
Fmr1
Dendritic spine
Dendrite
Layer V
Layer 5
Pyramidal neuron
Cerebral cortex
Mosaic
Cell-autonomous

ABSTRACT

Fragile X syndrome (FXS) is the most common form of intellectual disability that arises from the dysfunction of a single gene—*Fmr1*. The main neuroanatomical correlate of FXS is elevated dendritic spine density on cortical pyramidal neurons, which has been modeled in *Fmr1*$^{-/Y}$ mice. However, the cell-autonomous contribution of *Fmr1* on cortical dendritic spine density has not been assessed. Even less is known about the role of *Fmr1* in heterozygous female mosaic mice, which are a putative model for human *Fmr1* full mutation carriers (*i.e.*, are heterozygous for the full *Fmr1*-silencing mutation). In this neuroanatomical study, spine density in cortical pyramidal neurons of *Fmr1*$^{+/-}$ and *Fmr1*$^{-/Y}$ mice was studied at multiple subcellular compartments, layers, and brain regions. Spine density in *Fmr1*$^{+/-}$ mice is higher than WT but lower than *Fmr1*$^{-/Y}$. Not all subcellular compartments in layer V *Fmr1*$^{+/-}$ and *Fmr1*$^{-/Y}$ cortical pyramidal neurons are equally affected: the apical dendrite, a key subcellular compartment, is principally affected over basal dendrites. Within apical dendrites, spine density is differentially affected across branch orders. Finally, identification of FMRP-positive and FMRP-negative neurons within *Fmr1*$^{+/-}$ permitted the study of the cell-autonomous effect of *Fmr1* on spine density. Surprisingly, layer V cortical pyramidal spine density between FMRP-positive and FMRP-negative neurons does not differ, suggesting that the regulation of the primary neuroanatomical defect of FXS—elevated spine density—is non-cell-autonomous.

1. Introduction

Fragile X Syndrome (FXS) is the most common form of intellectual disability caused by a single gene mutation of *Fmr1*. FXS causes a wide array of symptoms ranging from intellectual disability to anxiety and autism (Hagerman et al., 2017). The behavioral phenotype of FXS often involves hyperarousal to sensory stimuli (Rais et al., 2018). The severity of this disorder appears to be correlated with the degree of Fragile X Mental Retardation Protein (FMRP) deficiency. FXS is an X-linked chromosomal disorder presenting mostly in males, but female *Fmr1* full mutation carriers (who are heterozygous for the full *Fmr1*-silencing mutation) possess a mosaic of FMRP-positive and FMRP-negative cells in their brain tissue (Rifé et al., 2004) due to random X-chromosome inactivation, leading to a high range (Reiss et al., 1995) of intellectual disabilities that are somewhat milder than in FXS (Turner et al., 1980).

Neurons, circuits, and behaviors are all perturbed due to loss of FMRP expression, including hyperexcitability that is associated with altered dendritic spine density (Contractor et al., 2015). Dendritic spines are protrusions on apical and basal dendrites of neurons and consist of the postsynaptic component of excitatory synapses. Dendritic spine density is directly associated with synaptic density onto excitatory pyramidal neurons (Arellano et al., 2007). Previous studies performed on postmortem tissue from donors with FXS indicate that dendritic spine density is higher when compared to tissue from age-matched controls (Irwin et al., 2001). This effect is paralleled within FXS model mice, in which *Fmr1* is knocked out (Bakker et al., 1994). Specifically, apical dendrites within layer V occipital cortex of *Fmr1*$^{-/Y}$ mice display an increased dendritic spine density and increased total spine length (Comery et al., 1997). Both a cell-autonomous astrocytic role and a cell-autonomous presynaptic role for *Fmr1* in regulating spine density of pyramidal neurons in layer V mouse motor cortex and mouse hippocampus have been identified, respectively (Hodges et al., 2017; Hanson

* Corresponding authors.
E-mail addresses: yizuo@ucsc.edu (Y. Zuo), vidalgx@jmu.edu (G.S. Vidal).
[1] These authors contributed equally to this work.

https://doi.org/10.1016/j.nbd.2021.105253
Received 31 October 2020; Received in revised form 15 December 2020; Accepted 4 January 2021
Available online 6 January 2021

and Madison, 2007).

Most prior studies have focused exclusively on *Fmr1*$^{-/Y}$ mice, as they model the most severe form of FXS. Little is known regarding the functional role of FMRP within *Fmr1* full mutation carriers, of which heterozygous *Fmr1*$^{+/-}$ mice may be a model. In *Fmr1*$^{+/-}$ mosaics, it is unknown whether FMRP has any function for regulating cortical dendritic spine density, let alone its cell-autonomous and post-synaptic functions in this regard. This study compares *Fmr1*$^{+/-}$ to WT and *Fmr1*$^{-/Y}$ mice, revealing that *Fmr1*$^{+/-}$ mosaics have a neuroanatomical deficit that is milder than *Fmr1*$^{-/Y}$ mice, that *Fmr1* regulation of spine density is concentrated in certain subcellular compartments, and that FMRP may have a non-cell-autonomous function in regulating cortical dendritic spine density.

2. Materials and methods

2.1. Ethics statement

This study was carried out in accordance with all United States National Institutes of Health and Department of Agriculture guidelines for animal research and the Guide for the Care and Use of Laboratory Animals of the United States National Research Council. Protocols for this study were approved by the Institutional Animal Care and Use Committees of the University of California Santa Cruz and James Madison University.

2.2. Animals, husbandry, housing, and genotyping

The *Fmr1*$^{-/Y}$ mouse line (Bakker et al., 1994) was provided by The Jackson Laboratory (B6.129P2-*Fmr1*^{tm1Cgr}/J, #003025) and Dr. Steven T. Warren, Emory University. The GFP-M line (Feng et al., 2000) was obtained from The Jackson Laboratory (STOCK Tg(Thy1-EGFP)MJrs/J; #007788). These congenic strains were maintained on a C57BL6/J genetic background.

Male GFP-M line mice were bred with female *Fmr1*$^{+/-}$ mice to obtain wildtype males and females, *Fmr1* hemizygous males, and *Fmr1* heterozygous females. Approximately half the offspring expressed the GFP transgene and were used for this study.

Mice were housed in a standard laboratory vivarium with their parents and littermates until weaning (approximately postnatal day 21; P21). Offspring remained with their same-sex littermates until the experimental end point (P30 or P120). Mice were kept in a temperature and humidity-controlled environment with a 12-h light/dark cycle and had access to food and water *ad libitum*.

Every breeder and animal used for the study was genotyped. Tissue was collected by ear punch. Genotyping for the University of California, Santa Cruz colony was done using The Jackson Laboratory (Bar Harbor, ME) PCR protocols #25410 (for the *Fmr1* targeted mutation) and #25728 (for the GFP-M transgene). Genotyping for the James Madison University colony was done *via* Transnetyx (Cordova, TN), an automated real-time PCR genotyping provider, using the following probes: “Fmr1 WT,” “Fmr1 KO,” and “Thy1-3 Tg”.

2.3. Histology

At P30 or P120, animals were anesthetized with a lethal intraperitoneal injection of ketamine (400 mg/kg)-xylazine (40 mg/kg) or ketamine (240 mg/kg)-xylazine (48 mg/kg)-acepromazine (1.85 mg/kg), then perfused transcardially with phosphate buffered saline (PBS) followed by 4% paraformaldehyde (PFA) in PBS. Brains were immediately removed and post-fixed in 4% PFA at 4 °C overnight. Brains were then incubated for 2 days in a cryoprotective solution consisting of 30% sucrose and 0.05% sodium azide in Tris-buffered saline (TBS). Whole brains were then mounted to a slicing chuck using OCT compound (Tissue-Tek) and sectioned in the coronal plane on a Leica CM3050-S cryostat at a thickness of 40 μm.

For mosaic experiments, tissue was prepared as above, except that after post-fixation in 4% PFA, brains were transferred to 1% PFA and stored at 4 °C for at least 24 h. Each hemisphere was separated and embedded in 4% agar. A coronal cut was made across the rostral end of the brain. The brain was then mounted, rostral side down, onto a maneuverable stage of a Leica VT1000S vibrating microtome using cyanoacrylate glue. To our knowledge, a novel sectioning technique was employed that kept primary apical dendrites intact in every section as the brain was sectioned from visual cortex to somatosensory cortex. In visual cortex, layer V apical dendrites generally extend out from the cell soma laterally and caudally to the pia, whereas in somatosensory cortex, apical dendrites do not extend as caudally. To keep primary apical dendrites intact in all brain regions, each hemisphere was sectioned separately on an orientable magnetic specimen disc (Leica, #14046232060), at a thickness of 75 μm. This thickness was chosen to preserve the full primary apical dendrite while allowing the perisomatic FMRP expression of each neuron to be assessed. The orientation of the layer V apical dendrites in the sections was assessed with a fluorescence microscope. If necessary, the orientable specimen disc was then adjusted to keep apical dendrites parallel to the microtome’s blade. Adjustments were made approximately every 5 serial sections. Using this technique, the number of intact apical dendrites was maximized within each section.

2.4. Immunohistochemistry

Fluorescent immunohistochemistry was used to identify the fraction of GFP-positive neurons with perisomatic FMRP expression. Sections were rinsed three times in TBS (10 min per rinse), followed by blocking in 10% normal goat serum and 0.5% Triton-X in TBS for one hour at room temperature. Sections were incubated in rabbit anti-FMRP primary antibody (Abcam, 1:1000) overnight at 4 °C. Tissue was rinsed three times in TBS, then incubated in Alexa Fluor 594-conjugated goat anti-rabbit secondary antibody (Invitrogen, 1:1000) for 2 h at room temperature. Sections were then rinsed three times in TBS and mounted on glass slides with Fluoromount-G (Southern Biotech).

Chromogenic immunohistochemistry was used to analyze dendritic spines in GFP-positive neurons. Sections were rinsed and blocked as above, then incubated in rabbit anti-GFP primary antibody (Abcam, 1:5000) overnight at 4 °C. Tissue was rinsed in TBS before incubation in biotinylated goat anti-rabbit secondary antibody (Vector Labs, 1:400) for 1 h at room temperature. Tissue was rinsed three times in TBS before incubation in the avidin/biotin-based peroxidase system (VECTASTAIN Elite ABC system, Vector Labs) for 1 h at room temperature, rinsed three times in TBS and incubated in DAB (3,3′-diaminobenzidine peroxidase substrate kit, Vector Labs) for approximately 2 min. Sections were rinsed three times in TBS, mounted onto glass slides, dried, and dehydrated in ethanol solutions of increasing concentration (50%, 70%, 95%, 100%, 100% EtOH, 3 min each) followed by clearing twice with xylenes (3 min each). Sections were covered in DPX Mounting Medium (Electron Microscopy Sciences) before applying coverglass.

For mosaic experiments, double fluorescent immunohistochemistry was used to enhance the green fluorescence of GFP-positive neurons for dendritic spine analysis (Bland et al., 2017) and to determine each neuron’s perisomatic expression of FMRP. Antigen retrieval was done by incubating sections in 10 mM sodium citrate buffer, pH 6.0 with 0.05% Tween-20 (vol/vol) at 85 °C for 20 min. Sections were then rinsed with PBS and then incubated in a blocking solution of 5% normal horse serum (vol/vol) and 0.01% Triton-X (vol/vol) in PBS for 30 min at room temperature. Tissue was incubated in primary antibody solution consisting of rabbit anti-GFP antibody (Novus Biologicals, 1:100) and mouse FMRP 2F5-1 antibody (DSHB, 1:1) at 4 °C for 16 h. Sections were incubated in horse anti-mouse Dylight 594 (Vector Labs, 1:200) and horse anti-rabbit Dylight 488 (Vector Labs, 1:200) at room temperature for 2 h, rinsed in PBS, and mounted onto glass slides with ProLong Diamond (Invitrogen).

2.5. Cell classification, imaging, and analysis

To identify the fraction of GFP-positive neurons with perisomatic FMRP expression in fluorescently-stained sections, neurons from 1 or 4 month old WT, *Fmr1*$^{-/Y}$ and *Fmr1*$^{+/-}$ mice were visualized using a Zeiss Axio Imager.M2 microscope. Stereo Investigator software (MBF Bioscience) was used to mark and quantify cells. GFP-positive neurons that showed any perisomatic FMRP labeling were counted as FMRP-positive. The experimenter was blind to all genotypes until all analysis was complete. Confocal image examples (Fig. 1A) were acquired on a Leica SP5 confocal system with a 20×/0.75NA objective.

In chromogenically-stained sections, layer V pyramidal neurons were imaged and traced using a Zeiss Axio Imager.M2 microscope with a 63×/1.4NA oil immersion objective, and contrast was enhanced by differential interference contrast microscopy. The microscope was equipped with a digital camera (AxioCam MRc, Zeiss), motorized stage and x-y-z encoder. The computer dedicated to this microscope was equipped with Neurolucida software (MBF Bioscience) which was used for tracing dendritic branches and spines. The primary somatosensory (barrel field) cortex, primary auditory cortex, primary visual cortex, and the CA1 region of hippocampus were identified by matching anatomical landmarks to a mouse brain atlas (Paxinos and Franklin, 2004). Simple cells of layer V were selected under low magnification based on their apical tuft branching pattern and integrity. GFP-immunolabeled apical dendritic tufts from layer V pyramidal neurons were traced from the primary dendrite (at a distance of approximately 100–150 μm deep to the pial surface) to their termination points; basal dendrites branching directly off the cell body were traced from the soma to their termination points. Any dendritic segments ≤2 μm in length were omitted from analysis. Layer II/III pyramidal neurons were traced similarly, and apical and basal dendritic segments of CA1 hippocampal neurons of 100 μm or longer were also traced similarly. Reconstructed dendritic data from chromogenically-stained neurons were analyzed using NeuroExplorer (MBF Bioscience), and branch order was assigned centrifugally (*i.e.*, primary dendrites arise from the soma, after branching and when they branch, secondary dendrites follow).

For mosaic experiments, sections were imaged with a Nikon TE2000 widefield and C2si laser scanning confocal microscope, using 10×/0.45NA and 60×/1.4NA objectives. A 60× image was taken of the cell soma to determine the presence of FMRP (red; 561 nm excitation) in GFP-positive layer V pyramidal neurons (green; 488 nm excitation), scanned sequentially to avoid any cross-channel interference. GFP-

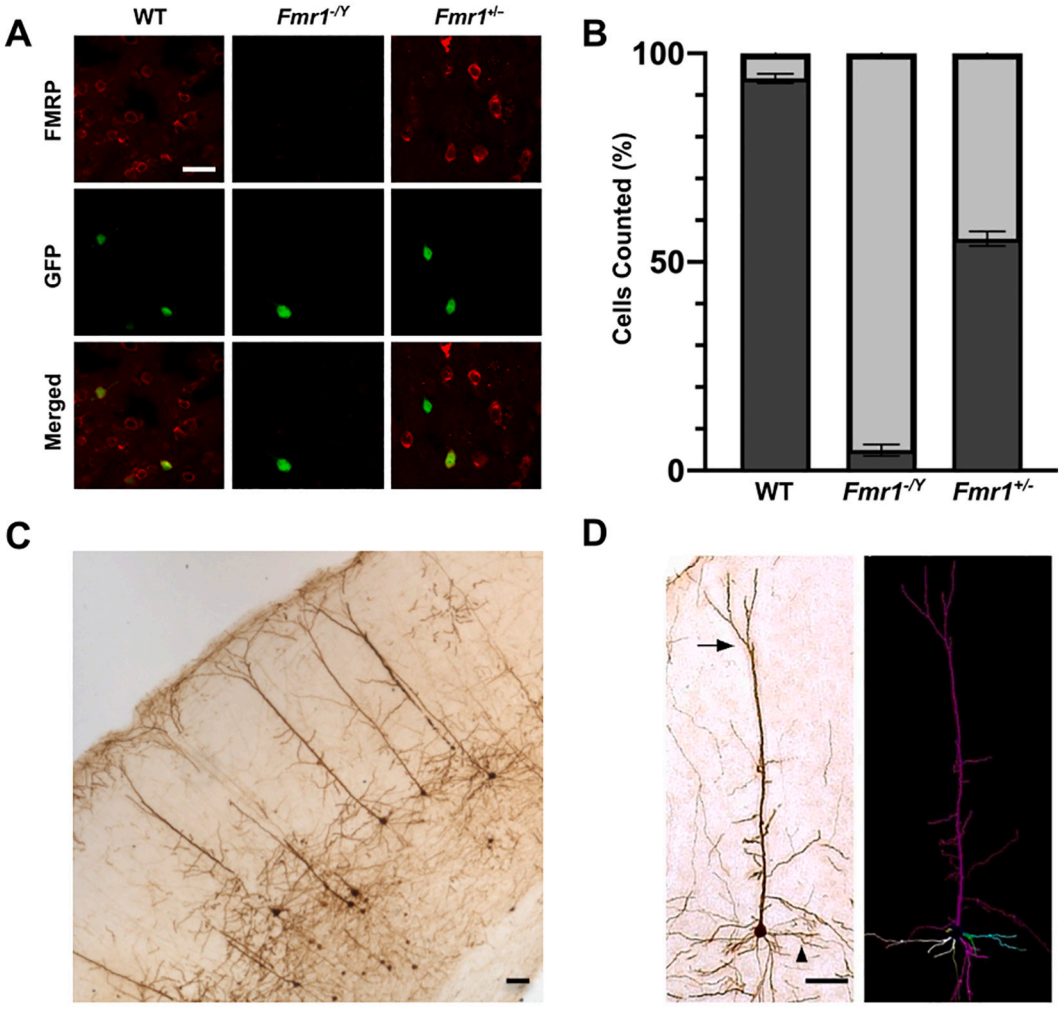

Fig. 1. FMRP expression patterns in WT, *Fmr1*$^{-/Y}$, and *Fmr1*$^{+/-}$ mice. (A) Medium magnification immunofluorescent images showing FMRP labeling (red) and GFP-expressing layer V pyramidal neurons (green) in the barrel cortex of P30 WT, *Fmr1*$^{-/Y}$, and *Fmr1*$^{+/-}$ mice. **(B)** Percentage of GFP-expressing layer V pyramidal neurons with (dark grey) or without (light grey) FMRP labeling. WT: 94.0 ± 1.1% FMRP positive, $N = 763$ neurons, 5 mice (3 male, 2 female). *Fmr1*$^{-/Y}$: 5.0 ± 1.4% FMRP positive, $N = 566$ neurons, 4 mice. *Fmr1*$^{+/-}$: 55.6 ± 1.7% FMRP positive, $N = 1037$ neurons, 5 mice. **(C)** Medium magnification image of GFP-positive, chromogenically-labeled layer V cortical pyramidal neurons. **(D)** Medium magnification image of chromogenically-labeled, GFP-positive layer V pyramidal neuron in the barrel cortex with apical dendrites (arrow), basal (arrowhead) dendrites (left), and reconstruction (right). Scale bars: 50 μm (A), 40 μm (C), 50 μm (D).

positive neurons that exhibited any perisomatic FMRP labeling within the cell body were counted as FMRP-positive. Then, the apical dendrite was followed manually at 60× until the primary branch point was reached. The primary and secondary dendrites around the branch point were imaged at 60× at the Nyquist sampling rate in the x, y, and z directions. Only neurons that exhibited a complete and intact apical dendrite were imaged and analyzed. Images from layer V cerebral cortical pyramidal neurons were classified into brain regions, which were identified by registering coronal sections to the Allen Mouse Brain Atlas (2004; Lein et al., 2007). An even distribution of neurons in primary visual cortex, primary somatosensory cortex, and primary auditory cortex were collected for analysis. Dendritic spines along the last 40 μm of dendrite before the primary branch point of layer V apical dendrites were counted using FIJI software (Schindelin et al., 2012; Rueden et al., 2017). Dendritic spine type was classified as mushroom, stubby, or thin (Harris et al., 1992) by using automatic detection NeuronStudio software based on Rayburst sampling (Rodriguez et al., 2006; Rodriguez et al., 2008) and was followed by manual analysis to eliminate false positives and negatives. Automatic detection of dendritic spines followed by manual correction is a method shown to reduce subjectivity and variability (Rodriguez et al., 2008). Statistical tests used here have been shown to reduce false positive and negative statistical errors in dendritic spine morphology analysis (Ruszczycki et al., 2012).

In all cases, dendritic spines were defined as any visible protrusion on the dendrites of traced segments, and spine density was defined as the total number of dendritic spines counted on a given dendrite divided by the total length of the segment. All statistical tests were performed using GraphPad Prism software. Unless otherwise noted, all grouped data are presented as mean ± SEM.

3. Results

3.1. Random X-chromosome inactivation among pyramidal neurons of *Fmr1*$^{+/-}$ mice

To approximate the X-chromosome inactivation ratio and pattern in *Fmr1*$^{+/-}$ mice, 2366 GFP-positive neurons were immunostained and analyzed for FMRP expression in the barrel field of the mouse somatosensory cortex of *Fmr1*$^{+/-}$ mosaics and controls (Fig. 1A). To do so, the GFP-M line was crossed with the loss-of-function *Fmr1* targeted mutation to generate three *Fmr1* genotypes: WT (serving as a positive control), *Fmr1*$^{-/Y}$(serving as a negative control), and *Fmr1*$^{+/-}$. Animals from the GFP-M line mostly express GFP sparsely among cortical layer V pyramidal neurons and in the CA1 region of the hippocampus (Feng et al., 2000). GFP-positive neurons in the somatosensory cortex of WT mice expressed FMRP (94.0 ± 1.1%; Fig. 1B). Conversely, only a very small fraction of neurons in the *Fmr1*$^{-/Y}$ appeared to express FMRP (5.0 ± 1.4%; Fig. 1B), which may represent the false positive rate of utilizing immunohistochemistry as an approximate measure of X-chromosome inactivation ratio. In *Fmr1*$^{+/-}$, approximately half of GFP-positive neurons also expressed FMRP (55.6 ± 1.7%; Fig. 1B). There was no discernible pattern of distribution or intensity of FMRP staining in FMRP-positive neurons in the cortex (Fig. 4A, K). Within FMRP-positive neurons, most FMRP was concentrated perisomatically and in primary dendrites (Fig. 1A).

3.2. Elevated apical dendritic spine density of layer V pyramidal neurons in *Fmr1*$^{-/Y}$ and *Fmr1*$^{+/-}$ mice across multiple primary sensory regions

A key, consistent neuroanatomical finding in the adult *Fmr1*$^{-/Y}$ mouse is elevated dendritic spine density of layer V cortical pyramidal neurons (He and Portera-Cailliau, 2013). Hypersensitivity to auditory, somatosensory, and visual stimuli is a characteristic trait of Fragile X Syndrome (Rais et al., 2018), which could be mediated by aberrant structural changes in the primary auditory, somatosensory, and visual cortex, respectively. To analyze dendritic spine density in these regions, GFP-positive layer V pyramidal neurons from WT, *Fmr1*$^{-/Y}$, and *Fmr1*$^{+/-}$ mice were chromogenically stained for GFP. Stained tissue is sparsely labeled and high-contrast (Fig. 1C), permitting individual layer V pyramidal neurons to be identified across multiple brain regions, and their apical and basal dendrites to be accurately imaged and traced (Fig. 1D). Layer V pyramidal neurons from the primary auditory (A1), primary somatosensory (S1), and primary visual (V1) regions were traced. Apical spine density in *Fmr1*$^{-/Y}$ mice is 59–84% higher than WT across all three primary sensory regions of the cortex sampled (Fig. 2D, I, N, Q, Table 1).

In *Fmr1*$^{+/-}$ mice, apical dendritic spine density is 36–47% higher than WT across all three primary sensory regions (Fig. 2D, I, N, Q, Table 1; in the case of A1, $p = 0.05$).

Within each genotype, mean apical and basal spine density was compared across the three sampled brain regions (Fig. 2P). Mean spine density generally does not vary across multiple brain regions within each genotype (Fig. 2P). Only 1 out of 18 statistical comparisons revealed a difference in the means for unknown reasons (apical but not basal spine density in S1 *vs.* V1 within *Fmr1*$^{+/-}$ mosaics, Fig. 2P). In all other cases, apical dendritic spine density does not vary across brain regions within each genotype. Basal dendritic spine density is also invariant across brain regions within each genotype.

Next, the overall cortical apical and basal spine densities of WT, *Fmr1*$^{-/Y}$, and *Fmr1*$^{+/-}$ mice were compared (Fig. 2Q). Combining the data in this way revealed that the mean apical spine density on *Fmr1*$^{+/-}$ mice differs from both WT and *Fmr1*$^{-/Y}$ (Fig. 2Q). In other words, the mean apical spine density of *Fmr1*$^{+/-}$ mice is between that of WT and *Fmr1*$^{-/Y}$.

In Golgi-Cox studies of the layer V pyramidal neurons of rats, dendritic spine density is known to vary along the length of the apical dendrite. For example, peak apical spine density is generally observed along the compartments of apical dendrite that pass from layer IV into layer II/III. As the apical dendrite approaches the cortical surface, dendritic spine density gradually decreases (Kunz et al., 1972; Michalski et al., 1976; Schönheit and Schulz, 1976). This pattern is particularly prominent when considering the branch orders of the apical dendrites. For example, in apical dendritic tufts of rat layer V pyramidal neurons, primary apical dendrites have the highest dendritic spine density, and spine density decreases gradually along secondary and higher-order apical dendrites (Schönheit and Schulz, 1976; Michalski et al., 1976). In chromogenically-stained sections of GFP-labeled layer V pyramidal neurons of mouse cortex (Fig. 3A), it was possible to reconstruct the entire neuron (Fig. 3A) and assign a branch order to each segment of apical (Fig. 3B) and basal dendrites (Fig. 3C). In all genotypes, apical dendritic spine density along layer V cortical pyramidal neurons gradually decreases with increasing branch order (Fig. 3D). For example, in WT, apical spine density begins at 0.94 ± 0.04 spines/μm at the primary dendrite, then decreases 23% to 0.72 ± 0.03 spines/μm at the secondary dendrites, and continues decreasing in higher branch orders (down to 0.55 ± 0.04 spines/μm in quinary dendrites, representing a 41% decrease from primary apical spine density; Fig. 3D, Supplemental Table 1).

A similar pattern exists in both *Fmr1*$^{-/Y}$ and in *Fmr1*$^{+/-}$, though their overall spine density is higher (Fig. 3D). In fact, a two-way ANOVA of the apical dendritic spine density data shown in Fig. 2D reveals that dendritic order and genotype account for 35% and 18% of the total variation in the sample, respectively ($p < 0.0001$ for dendritic order and for genotype). Interaction between the genotype and dendritic order was also found ($p < 0.0001$), though it only accounts for 3% of the total variation in the sample and is likely not biologically relevant. Tukey multiple comparisons show that both *Fmr1*$^{-/Y}$ and *Fmr1*$^{+/-}$ differ from WT at every branch order tested ($p < 0.0001$ in primary, secondary, and tertiary dendrites; $p < 0.005$ in quaternary dendrites, and $p < 0.02$ in quinary dendrites).

At the primary apical dendrite, *Fmr1*$^{+/-}$ differ from both WT and *Fmr1*$^{-/Y}$ ($p < 0.0001$). In this case, *Fmr1*$^{+/-}$ primary apical dendritic spine density is 1.32 ± 0.06 spines/μm, which is 40% higher than WT

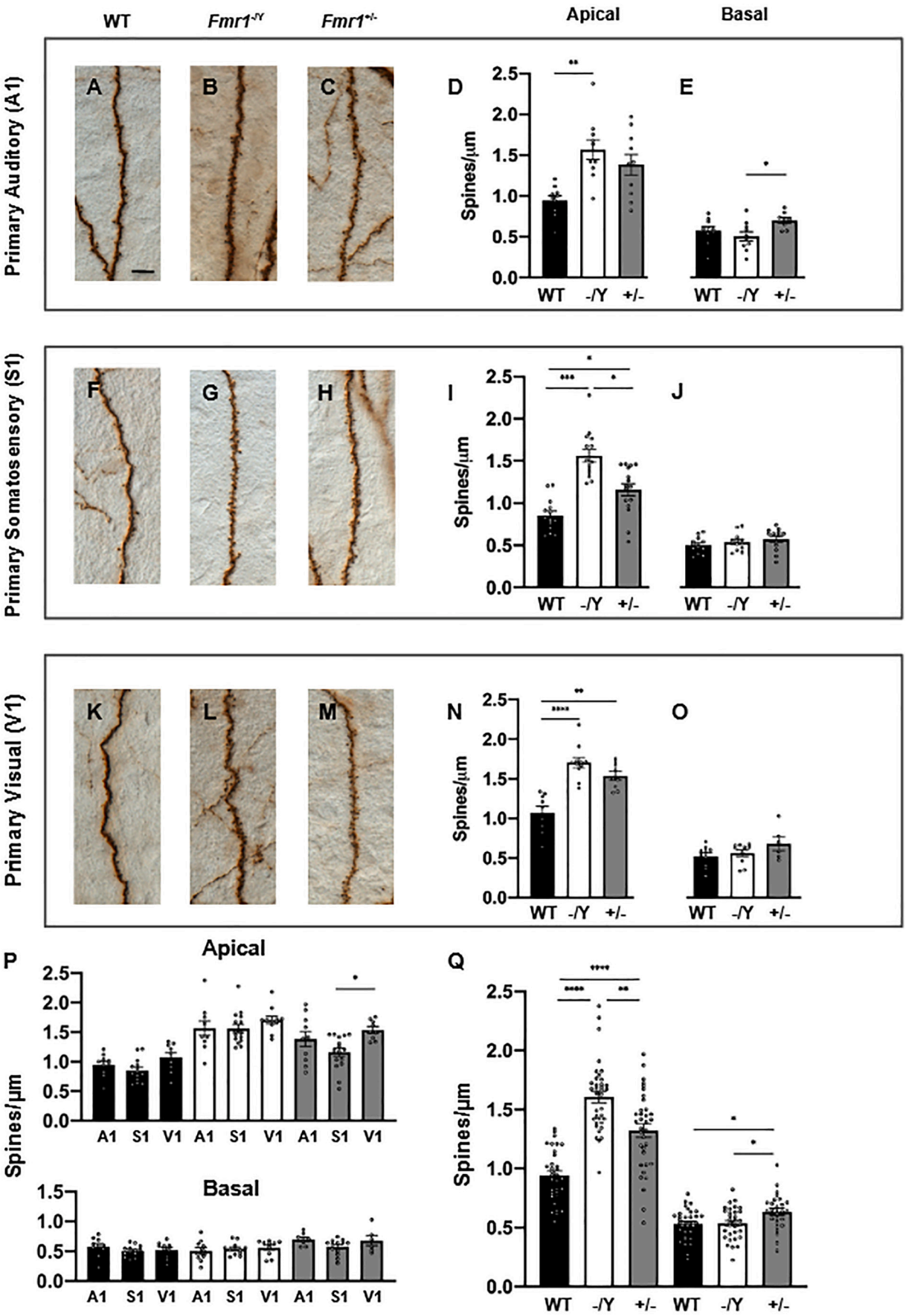

(caption on next page)

Fig. 2. Dendritic spine densities of apical layer V pyramidal neurons in adult *Fmr1*$^{-/Y}$and *Fmr1*$^{+/-}$mice are significantly elevated when compared to WT across multiple cortical regions. (A-C) High magnification (63×) photomicrographs of chromogenically-labeled apical dendrites from GFP-positive layer V pyramidal neurons in primary auditory cortex (A1) of WT, *Fmr1*$^{-/Y}$, and *Fmr1*$^{+/-}$ mice. **(D)** Spine density of apical dendrites from layer V pyramidal neurons in primary auditory cortex of WT, *Fmr1*$^{-/Y}$ (−/Y), and *Fmr1*$^{+/-}$ (+/−) mice. **(E)** as in D, but of basal dendrites. **(F–J)** as in A-E, but in primary somatosensory (barrel, S1) cortex. **(K–O)** as in A-E, but in primary visual cortex (V1). **(P)** Summary of data presented in panels D, E, I, J, N, and O, grouped by genotype. **(Q)** Grouped dendritic spine density data from neurons in all three regions. Statistics: Mann-Whitney tests with Dunn's multiple comparisons (comparing across genotypes, except in panel P, which compare across cortical regions), * $p < 0.05$, ** $p < 0.01$, *** $p < 0.001$, **** $p < 0.0001$.

Table 1
P-values, mean spine density, and N for Fig. 2.

Figure	WT *vs.* *Fmr1*$^{-/Y}$ *p-value*	WT *vs.* *Fmr1*$^{+/-}$ *p-value*	*Fmr1*$^{-/Y}$ *vs.* *Fmr1*$^{+/-}$ *p-value*	WT *mean spines/μm ± SEM; N (cells, mice)*	*Fmr1*$^{-/Y}$ *mean spines/μm ± SEM; N (cells, mice)*	*Fmr1*$^{+/-}$ *mean spines/μm ± SEM; N (cells, mice)*
2D	<0.01	0.05	>0.99	0.94 ± 0.06; 10, 5	1.57 ± 0.12; 10, 3	1.38 ± 0.13; 10, 4
2E	0.98	0.33	0.03	0.58 ± 0.05; 10, 5	0.51 ± 0.06; 10, 3	0.70 ± 0.04; 8, 4
2I	<0.001	<0.05	0.01	0.85 ± 0.05; 14, 4	1.56 ± 0.07; 15, 5	1.16 ± 0.07; 15, 5
2 J	>0.99	0.28	>0.99	0.50 ± 0.03; 13, 4	0.54 ± 0.03; 12, 5	0.57 ± 0.04; 13, 5
2 N	<0.0001	<0.01	0.77	1.07 ± 0.08; 9, 4	1.71 ± 0.06; 11, 4	1.54 ± 0.05; 9, 4
2O	>0.99	0.41	>0.99	0.52 ± 0.04; 10, 4	0.56 ± 0.04; 10, 4	0.68 ± 0.08; 6, 4
2Q (Apical)	<0.0001	<0.0001	<0.01	0.94 ± 0.04; 33, 5	1.61 ± 0.05; 36, 5	1.32 ± 0.06; 35, 5
2Q (Basal)	>0.99	0.02	0.03	0.53 ± 0.02; 33, 5	0.54 ± 0.02; 32, 5	0.63 ± 0.03; 27, 5

(0.94 ± 0.04 spines/μm), and 18% lower than *Fmr1*$^{-/Y}$ (1.60 ± 0.05 spines/μm; Fig. 3D, Supplemental Table 1). Overall, both *Fmr1*$^{+/-}$ and *Fmr1*$^{-/Y}$ have higher apical dendritic spine density at all branch orders (Supplemental Table 1).

3.3. Basal dendritic spine density of layer V cortical pyramidal neurons in WT, *Fmr1*$^{-/Y}$, and *Fmr1*$^{+/-}$ mice

Contrastingly, basal dendritic spine density of layer V cortical pyramidal neurons in *Fmr1*$^{-/Y}$ or *Fmr1*$^{+/-}$ is minimally altered when compared to WT (Fig. 2). The only exceptions appear to occur between *Fmr1*$^{+/-}$ and *Fmr1*$^{-/Y}$ in A1 ($p < 0.05$, Fig. 2E), or among WT, *Fmr1*$^{-/Y}$, and *Fmr1*$^{+/-}$ after data from all regions are combined ($p < 0.05$, Fig. 2Q). However, the difference in these means is small and may not be biologically relevant. For example, after pooling data across all sampled regions, only a 0.10 spine/μm difference exists among the mean basal dendritic spine density of the three genotypes (Fig. 2Q, Table 1).

In the case of basal dendrites (Fig. 3D), there is no biologically relevant effect of genotype or dendritic order on basal dendritic spine density (two-way ANOVA). In fact, only basal dendritic order is a statistically significant factor in spine density ($p = 0.02$) but it only accounts for 3% of the total variation in the sample. The primary basal dendrite is the only location where there is any difference across genotypes (*Fmr1*$^{+/-}$ differ from both WT and *Fmr1*$^{-/Y}$, but only by 0.10 spines/μm or less; $p < 0.008$, Tukey multiple comparisons; Fig. 3D).

3.4. Dendritic spine density of pyramidal neurons in region CA1 of hippocampus, in cortical layer II/III, and in cortical layer V of juvenile WT, *Fmr1*$^{-/Y}$, and *Fmr1*$^{+/-}$ mice

Fmr1 genotype is known to regulate dendritic spine density in pyramidal neurons outside layer V (He and Portera-Cailliau, 2013). In pyramidal neurons of the CA1 region of hippocampus, for example, genotype (but not dendritic order) accounts for 53% of the total variation in the sample of apical dendritic spine density ($p < 0.0001$, Supplemental Fig. 1, two-way ANOVA). In contrast to layer V cortical pyramidal neurons, the effect is not restricted to apical dendrites: genotype also accounts for 24% of the variation in basal dendrites of pyramidal neurons in CA1 ($p < 0.0001$, Supplemental Fig. 1). Finally, *Fmr1* genotype is not a significant variable affecting the dendritic spine density of layer II/III cortical pyramidal neurons (Supplemental Fig. 2). In layer II/III pyramidal neurons, dendritic order accounts for 40% and 32% of the total variation in apical and basal dendritic spine density, respectively ($p < 0.0001$, Supplemental Fig. 2, two-way ANOVA). In sum, *Fmr1* genotype is a relevant variable in pyramidal neurons of both CA1 of hippocampus and layer V of cortex, but only layer V cortical pyramidal neurons display a cell compartment-specific (apical) effect of *Fmr1* genotype.

Fmr1$^{-/Y}$ mouse models of Fragile X Syndrome characteristically show elevated dendritic spine density of layer V cortical pyramidal neurons by adulthood (He and Portera-Cailliau, 2013), which is known to occur because of an overproduction of new spines between 1 and 4 months of age (Hodges et al., 2017). Indeed, at 1 month of age, *Fmr1* genotype was not a significant variable in the dendritic spine density of layer V cortical pyramidal neurons (Supplemental Fig. 3, two-way ANOVA). In contrast, apical dendritic order at this age is already a significant variable for spine density ($p < 0.0001$), accounting for 48% of the total variation in the sample (two-way ANOVA). Even basal dendritic order was already a significant variable for spine density at this age ($p = 0.03$, 14% of total variation, two-way ANOVA).

3.5. In *Fmr1*$^{+/-}$ mice, apical dendritic spine density defect in layer V cortical pyramidal neurons is not cell-autonomous

In *Fmr1*$^{+/-}$ mice crossed to the GFP-M line, approximately half of GFP-positive layer V pyramidal neurons express FMRP perisomatically (Fig. 1A, B). The cell-specific effect of FMRP could be investigated in this mosaic model by using double fluorescent immunohistochemistry to determine the FMRP expression of each neuron and by preserving the integrity of the primary apical dendrite during sectioning. To validate the method, primary apical dendritic spine density in *Fmr1*$^{+/-}$ were first compared to WT and *Fmr1*$^{-/Y}$ prepared the same way. As expected, all GFP-positive neurons in WT tissue expressed FMRP perisomatically (Fig. 4B–D), whereas no GFP-positive neurons in *Fmr1*$^{-/Y}$ tissue expressed FMRP (Fig. 4G–I). In *Fmr1*$^{+/-}$, GFP-positive neurons both with perisomatic FMRP expression (Fig. 4L–N) and without it (Fig. 4P–R) could be identified, as expected (Fig. 1A, B). In all three genotypes (WT, *Fmr1*$^{-/Y}$, and *Fmr1*$^{+/-}$), both the FMRP expression (Fig. 4B–D, G–I, L–N, P–R) and the spine density of the primary apical dendrite of each GFP-positive neuron (Fig. 4E, J, O, S) were observed.

Fmr1 genotype was a major determinant of primary apical dendritic spine density (Fig. 4T, Kruskal-Wallis $p = 0.006$). Primary apical dendritic spine density of layer V cortical pyramidal neurons of *Fmr1*$^{-/Y}$ (1.25 ± 0.09 spines/μm, Fig. 4T) was 42% greater than WT (0.88 ± 0.12 spines/μm, Dunn's multiple comparisons $p = 0.04$). Similarly, primary apical dendritic spine density in *Fmr1*$^{+/-}$ (1.31 ± 0.08 spines/μm,

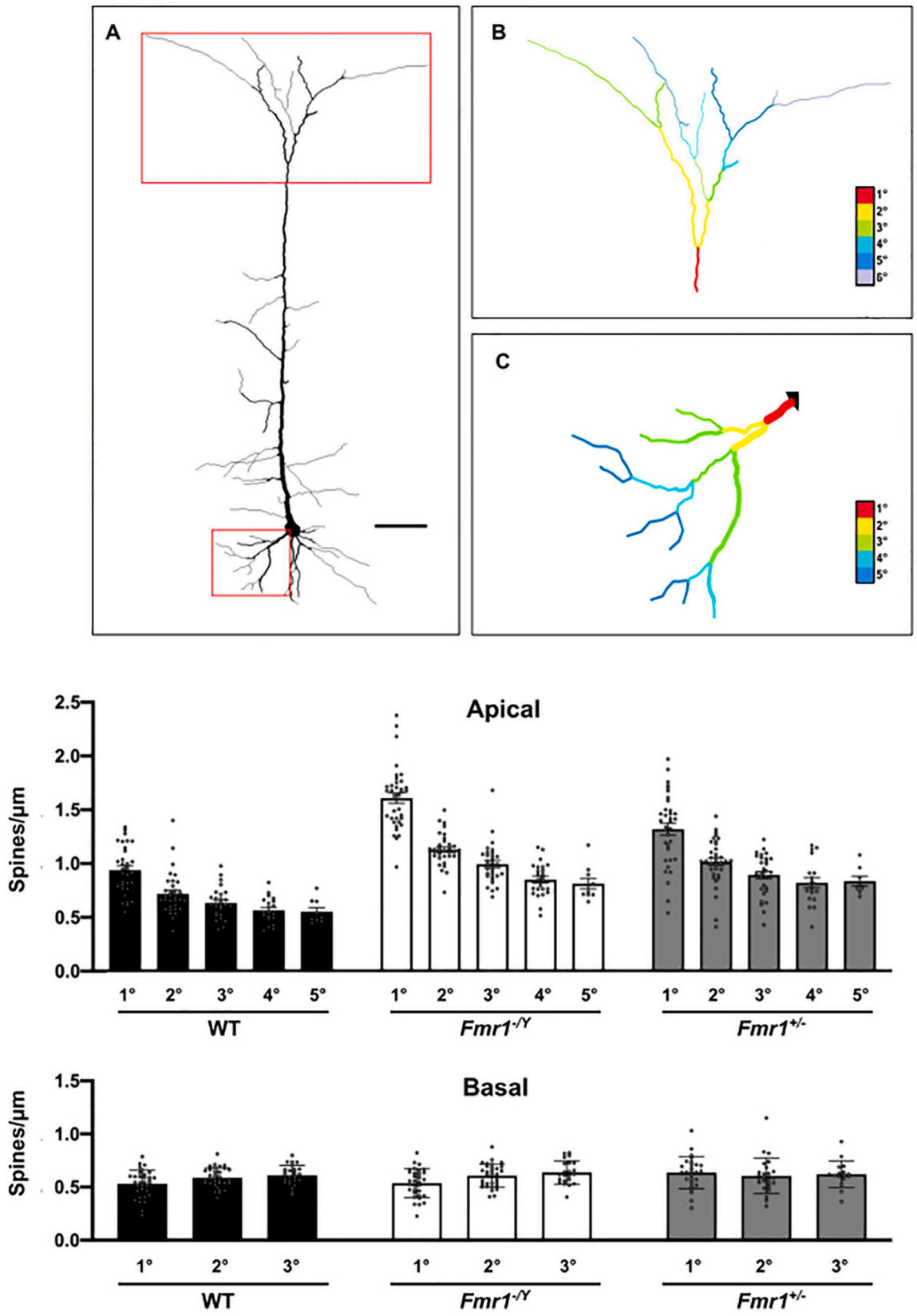

Fig. 3. Dendritic spine densities in apical but not basal layer V pyramidal neurons vary by genotype and branch order. (A) Camera lucida-style rendering of dendrites and soma of a layer V pyramidal neuron in barrel cortex (scale bar: 50 µm). **(B)** Dendritic branch orders of the apical dendritic tuft in (A). **(C)** Dendritic branch orders of a basal dendritic tree in (A). **(D)** Dendritic spine density in apical (top) and basal (bottom) dendrites from sensory cortex (sampled from A1, S1, V1), according to branch order and genotype. See Supplemental Table 1 for mean spines/µm ± SEM and N (cells, mice).

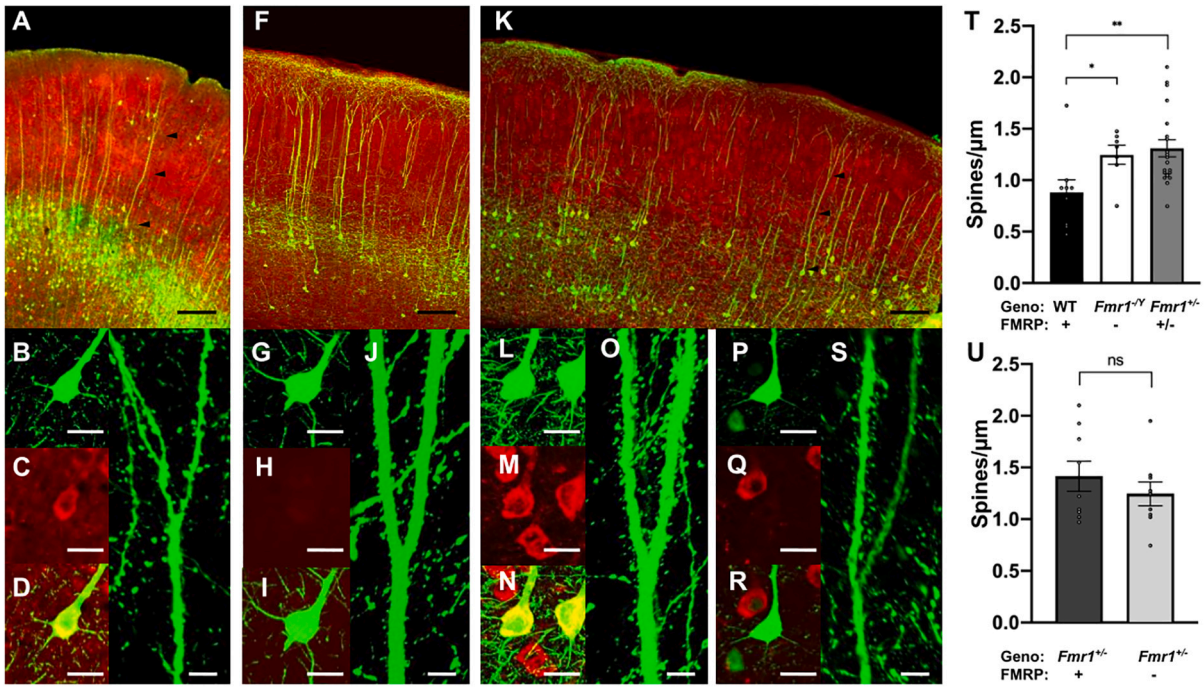

Fig. 4. Elevated primary apical dendritic spine density in *Fmr1*$^{+/-}$mice. (A) Low-magnification view (10×) of GFP-positive (green) and FMRP-positive cortical cells (red) from WT tissue. A layer V pyramidal neuron with an intact primary apical dendrite is identified by arrowheads. Cortical surface is at the top and layer V is delineated by somatic GFP labeling. **(B)** Magnified confocal view (60×) of WT tissue in (A), showing somatic GFP labeling of layer V pyramidal neuron. GFP-labeled apical dendrite is to the top right of the soma. **(C)** Perisomatic FMRP labeling of pyramidal neuron in (B). **(D)** Composite image of (B) and (C). **(E)** Primary (bottom) dendrite and secondary dendrites (top) of pyramidal neuron in B–D. **(F–J)** As in A-E, but in *Fmr1*$^{-/Y}$ tissue. **(K)** As in (A) but in *Fmr1*$^{+/-}$ tissue. **(L–O)** As in (B-E), but an FMRP-positive neuron in *Fmr1*$^{+/-}$ tissue. **(P–S)** As in (B-E), but an FMRP-negative neuron in *Fmr1*$^{+/-}$ tissue. **(T)** Comparison of primary apical spine density in layer V cortical pyramidal neurons of WT, *Fmr1*$^{-/Y}$, and *Fmr1*$^{+/-}$ mice. N (WT, *Fmr1*$^{-/Y}$, *Fmr1*$^{+/-}$) = 7 neurons (1 mouse), 9 neurons (1 mouse), 18 neurons (5 mice). **(U)** Data from *Fmr1*$^{+/-}$ as in (T) but split into FMRP-positive and FMRP-negative neurons. N (FMRP-positive, FMRP-negative) = 9, 9 neurons from 5 mice. Scale bars: 50 µm (A, F, K), 20 µm (B–D, G–I, L–N, P–R), 5 µm (E, J, O, S).

Fig. 4T) was 49% higher than primary apical dendritic spine density in WT (Dunn's multiple comparisons $p = 0.007$). This result recapitulated the elevated dendritic spine density in layer V pyramidal neurons from *Fmr1*$^{-/Y}$ and *Fmr1*$^{+/-}$ tissue, when compared to WT (Fig. 2, Table 1, Fig. 3).

The higher primary apical spine density of layer V pyramidal neurons of *Fmr1*$^{+/-}$ compared to WT could result from two possibilities. One possibility is that *Fmr1* has a cell-specific, postsynaptic effect on spine density. In this case, FMRP-negative neurons would be expected to have a higher spine density than FMRP-positive neurons, much like layer V cortical pyramidal neurons of *Fmr1*$^{-/Y}$ have a higher spine density than WT. An alternative possibility is that the higher spine density in layer V neurons of *Fmr1*$^{+/-}$ is not caused by a cell-specific and postsynaptic effect of *Fmr1*. In this case, a difference in spine density between FMRP-negative and FMRP-positive neurons would not be expected.

No difference in spine density was observed between FMRP-positive and FMRP-negative layer V pyramidal neurons in *Fmr1*$^{+/-}$ (1.417 ± 0.14 spines/µm and 1.247 ± 0.11 spines/µm, respectively; Fig. 4U, $p > 0.05$, Mann-Whitney). Total dendritic spine density is a sum of all spine types: mushroom, stubby, and thin (Harris et al., 1992). It is possible for two neurons to have the same total spine density but have vastly different densities of each spine type. When testing for this possibility, no significant difference was found in mushroom, stubby, or thin spine density between FMRP-positive and FMRP-negative layer V pyramidal neurons (Supplemental Fig. 4, $p > 0.05$, two-way ANOVA).

4. Discussion

This neuroanatomical study revealed four major findings. First, X-chromosome inactivation appears to be randomly patterned in *Fmr1*$^{+/-}$ cortex, and X-chromosome inactivation ratio in the cortex is near 50% (Fig. 1). Second, *Fmr1* genotype is an important factor in regulating dendritic spine density across multiple primary sensory regions, even in *Fmr1*$^{+/-}$ (Fig. 2). To our knowledge, this study is the first to report dendritic spine abnormalities in the *Fmr1*$^{+/-}$ mosaic. Third, the apical dendrite of layer V cortical pyramidal neurons was identified as the subcellular compartment most associated with *Fmr1*-dependent changes in spine density (Fig. 3). Overall, the greatest neuroanatomical defect in this study was specifically found along the primary apical dendrite of layer V pyramidal cortical neurons in 4-month-old *Fmr1*$^{-/Y}$ and *Fmr1*$^{+/-}$ mice (70% and 40% increase in *Fmr1*$^{-/Y}$ and *Fmr1*$^{+/-}$ over WT, respectively; Fig. 3A, Supplemental Table 1). Finally, in *Fmr1*$^{+/-}$, postsynaptic FMRP expression does not appear to regulate spine density, even when focusing the investigation on the primary apical dendrite (Fig. 4).

This study also recapitulated some prior findings, including a high percentage of FMRP-expressing cortical pyramidal neurons in WT (94.0 ± 1.1%; Fig. 1B, see Hodges et al., 2017), FMRP expression around the soma and primary dendrites of cortical pyramidal neurons (Fig. 1A, see Feng et al., 1997), and *Fmr1*$^{-/Y}$ layer V pyramidal neurons had 59–84% higher apical spine density than WT in visual cortex (Fig. 2N, see Comery et al., 1997; McKinney et al., 2005) and somatosensory cortex (Fig. 2I, see Galvez and Greenough, 2005). *Fmr1* genotype is not a significant variable affecting the dendritic spine density of layer II/III cortical pyramidal neurons (Supplemental Fig. 2), which is in agreement with some (Meredith et al., 2007; Cruz-Martín et al., 2010) but not all (Dölen et al., 2007; Hayashi et al., 2007; Liu et al., 2011) studies, all of which were done on younger mice. In CA1, pyramidal neurons were affected by *Fmr1* genotype (Supplemental Fig. 1), recapitulating previous results (Levenga et al., 2011). Furthermore, dendritic spine type was not altered between FMRP-positive and FMRP-negative layer V

pyramidal neurons (Supplemental Fig. 4), which is in agreement with the prior finding that spine *type*, even in *Fmr1*$^{-/Y}$ mice, changes in an extremely subtle way during development (Wijetunge et al., 2014).

4.1. Non-cell-autonomous roles for FMRP in regulating spine density

Surprisingly, postsynaptic FMRP expression in layer V cortical pyramidal neurons from *Fmr1*$^{+/-}$ did not cause any detectable changes in spine density (Fig. 4U). Instead, neurons in the *Fmr1*$^{+/-}$ uniformly had higher spine density than WT controls (Fig. 4T, U). In other words, no postsynaptic, cell-autonomous function of FMRP in regulating dendritic spine density was observed in *Fmr1*$^{+/-}$. Thus, it is likely that FMRP exerts a non-cell-autonomous role on spine density of layer V cortical pyramidal neurons.

Other mosaic *Fmr1* studies have revealed cell-specific, presynaptic roles for FMRP in the developing brain. For example, presynaptic loss of *Fmr1* decreases connection probability in CA3 organotypic slice culture (Hanson and Madison, 2007). In another study, presynaptic *Fmr1* loss was linked to reduced excitation of layer IV fast-spiking inhibitory neurons in young (P13-16) *Fmr1*$^{+/-}$ mice, mimicking the phenotype of full *Fmr1*$^{-/Y}$ mice (Patel et al., 2013). Lastly, rescuing FMRP function within individually-patched pyramidal neurons in CA3 restored presynaptic action potential duration (Deng et al., 2013). Thus, a compelling future direction would be to determine the effect of presynaptic *Fmr1* genotype on dendritic spine density *in vivo*. This approach could determine whether or not supernumerary primary apical dendritic spines in layer V cortical pyramidal neurons of *Fmr1*$^{+/-}$ are mostly associated with presynaptic FMRP-negative neurons. FMRP is detectable in cortical neurons using histological preparations similar to our own (as presynaptic "granules": Christie et al., 2009; Akins et al., 2012). However, distinguishing between pre- and postsynaptic FMRP expression requires electron microscopy (Christie et al., 2009), conditional genetic approaches (Akins et al., 2012), or array tomography (Wang et al., 2016), as presynaptic FMRP is located less than 100 nm from the synaptic cleft (Wang et al., 2016). Alternatively, a way to test for a presynaptic role of FMRP in establishing apical dendritic spine density on layer V cortical pyramidal neurons would be to use an genetically encoded, X-linked fluorescent mouse line to label FMRP-positive neurons in mosaic tissue, as previously done *in vitro* in hippocampus (Hanson and Madison, 2007). At the same time, cell-specific, *postsynaptic* roles of FMRP have also been identified in the developing brain by using *Fmr1* models. For example, in the developing chick cochlear nucleus, selective loss of postsynaptic FMRP adversely affected neurotransmission and resulted in the abnormal development of presynaptic terminals (Wang et al., 2018). Lack of pruning of layer V to layer V excitatory synapses in somatosensory cortex of young *Fmr1*$^{-/Y}$ is thought to be postsynaptically-controlled (Patel et al., 2014). Restoring FMRP function in KO neurons of a young hippocampal slice culture leads to the elimination of spines (Pfeiffer and Huber, 2007, Pfeiffer et al., 2010). Finally, postsynaptic FMRP changes in young CA1 slices alterchange synapse number and maturity (Zang et al., 2013). FMRP is known to have multiple cellular roles (Davis and Broadie, 2017), which could be selectively increased or decreased during development and adulthood in different brain regions. For example, in the cerebral cortex, FMRP may have primarily cell-autonomous, postsynaptic roles during early development, but switch over to non-cell-autonomous roles in adulthood, as observed here.

Most (72%) excitatory synapses are apposed to an astrocytic process (Simhal et al., 2019), and astrocytic FMRP has been shown to be essential for normal circuit development in the cortex (Higashimori et al., 2016; Hodges et al., 2017). In fact, knocking out *Fmr1* from astrocytes alone can recapitulate the same dendritic spine abnormalities seen on pyramidal neurons from the full *Fmr1*$^{-/Y}$ (Hodges et al., 2017). Astrocytes undergo mitosis throughout life (Colodner et al., 2005), and progressive, preferential silencing of the *Fmr1* full mutation is known to occur in mitotic cells (Sun and Baumer, 1999). One intriguing possibility is that *Fmr1*$^{+/-}$ might have altered astrocytic X-chromosome inactivation ratios over time, leading to alterations in cortical circuitry. In humans, X-chromosome inactivation ratios in the blood of *Fmr1* full mutation carriers are known to be variable, even among sisters (Martínez et al., 2005), and the percent of leukocytes expressing FMRP is directly correlated with higher cognitive scores (de Vries et al., 1996; Loesch et al., 2004).

4.2. Consequences of Fmr1-mediated control of subcellular neuroanatomy

A major finding in this study was that *Fmr1* did not exert its effect on dendritic spine density equally among all subcellular compartments of pyramidal neurons (Fig. 3). Specifically, primary apical dendrites of layer V cortical pyramidal neurons were greatly affected, whereas basal dendrites were negligibly affected by *Fmr1*. An array tomography study analyzed synaptic density *Fmr1*$^{-/Y}$ and WT at the same brain region and age as this study (4-month-old somatosensory cortex) and found a much higher density of excitatory synapses (*via* array tomography) in layer IV over layer V of *Fmr1*$^{-/Y}$ (Wang et al., 2014). This neuroanatomical finding coincides with other models of neurological disorders that also lead to aberrant circuitry and behavior (Muhammad et al., 2012; Mychasiuk et al., 2013; Steele et al., 2014), but no common mechanistic relationship among these models has been tested yet.

It is well known that anatomically disparate compartments, such as apical and basal dendrites, receive distinct thalamocortical and corticocortical inputs (Petreanu et al., 2009; Rah et al., 2013). Relatedly, it is also known that *Fmr1*$^{-/Y}$ have disrupted interlaminar connectivity (Bureau et al., 2008), occurring much earlier than most *Fmr1*-mediated changes in spine density. An early disruption to interlaminar connectivity could lead to specific subcellular changes to dendritic spine density, occurring primarily at compartments receiving aberrant presynaptic connectivity. Finally, electrical properties such as dendritic diameter, length, and ion channel composition differ among dendritic compartments, and critical properties of the synapse, such as long-term synaptic plasticity, also differ (Kaibara and Leung, 1993). Major structural changes mediated by FMRP loss in one compartment over another could thus have multiple profound functional consequences on cortical circuitry.

4.3. Fmr1$^{+/-}$ mice and human Fmr1 full mutation carriers of Fragile X Syndrome

Human female carriers of the *Fmr1* full mutation generally have mild intellectual deficits (Turner et al., 1980; Uchida et al., 1983; Sherman et al., 1985; Hagerman et al., 1992; de Vries et al., 1996). In brains from FXS patients and from *Fmr1*$^{-/Y}$ model mice, the major neuroanatomical deficit is elevated dendritic spine density in pyramidal neurons. *Fmr1*$^{+/-}$ had a milder, but significant neuroanatomical deficit in layer V cortical pyramidal neurons, when compared to *Fmr1*$^{-/Y}$ (Fig. 2). FMRP expression in the cerebral cortex of human *Fmr1* full mutation carriers is "in roughly 50% of cortical cells without any specific pattern" (Rifé et al., 2004), similar to what was observed in this study in *Fmr1*$^{+/-}$ mice (Fig. 1). *Fmr1*$^{+/-}$ mice may be valuable for understanding cellular and circuit mechanisms by which intellectual deficits arise in human *Fmr1* full mutation carriers.

Here, approximately 55% of cortical pyramidal neurons in *Fmr1*$^{+/-}$ mice express FMRP, suggesting an even X-chromosome inactivation ratio. All *Fmr1*$^{+/-}$ mosaics in this study inherited the intact *Fmr1* gene paternally, meaning that 55% of neurons inactivated the *maternal* chromosome. However, it is known that the mouse brain has a small (6%) but significant skew toward inactivating the *paternal* X chromosome (Wang et al., 2010). This would suggest that the *Fmr1* mutation (inherited *maternally* in this study) may be preferentially silenced. Progressive, preferential silencing of the *Fmr1* mutation has been shown in cell culture, where fetal fibroblast tissue taken from full mutation

carriers incrementally expresses FMRP after each passage (Sun and Baumer, 1999). The degree to which preferential silencing occurs in mitotic neural progenitors of *Fmr1* full mutation carriers and *Fmr1*$^{+/-}$ is worth exploring because carriers present with a wide range of cognitive phenotypes (Reiss et al., 1995), possibly due to variations in FMRP mosaicism.

5. Conclusion

To our knowledge, this study is the first to report that *Fmr1*$^{+/-}$ mice have elevated apical dendritic spine density in layer V cortical pyramidal neurons, which is the primary neuroanatomical defect found in *Fmr1*$^{-/Y}$ mice and FXS patients. Postsynaptic FMRP expression in layer V pyramidal neurons of *Fmr1*$^{+/-}$ mice is not correlated with a cell-specific change in spine density, suggesting that FMRP regulates cortical dendritic spine density in a non-cell-autonomous manner.

Funding

This work was supported by grants from the National Institute of Neurological Disorders and Stroke (K01NS107723) to GV, the National Institute of Mental Health (R01MH109475 and R01MH104227) to YZ; startup by the James Madison University (JMU) Department of Biology to GV, a grant from 4-VA, a collaborative partnership for advancing the commonwealth of Virginia, to GV, a Virginia Academy of Sciences small research grant to GV, and by JMU College of Science and Mathematics Summer Faculty Assistance Grants to GV. Student support was generously provided by the JMU Department of Biology, a JMU College of Science and Mathematics Second Century Scholarship Summer Project Award to KB, Farrell scholarships (KB, ZC, BS), a Butler scholarship (KB), a Jeffrey E. Tickle '90 Family Endowment scholarship (ZLH and KB), and the JMU Second Century Scholarship (KB) and Centennial Scholarship (CH). Funding sources were not involved in study design, collection, analysis, interpretation, writing, or the decision to submit the article for publication.

Declaration of Competing Interest

None.

Acknowledgements

We thank Drs. Mark Gabriele and Marquis Walker for thoughtful feedback, Dr. Kris Kubow and the James Madison University Light Microscopy and Imaging Facility for use of the equipment and technical support, and Mses. Sarah Keegan and Stephanie Rubino for providing outstanding mouse care.

Appendix A. Supplementary data

Supplementary data to this article can be found online at https://doi.org/10.1016/j.nbd.2021.105253.

References

Akins, M.R., Leblanc, H.F., Stackpole, E.E., Chyung, E., Fallon, J.R., 2012. Systematic mapping of fragile X granules in the mouse brain reveals a potential role for presynaptic FMRP in sensorimotor functions. J. Comp. Neurol. 520, 3687–3706. https://doi.org/10.1002/cne.23123.

Arellano, J.I., Espinosa, A., Fairén, A., Yuste, R., DeFelipe, J., 2007. Non-synaptic dendritic spines in neocortex. Neuroscience 145, 464–469. https://doi.org/10.1016/j.neuroscience.2006.12.015.

Bakker, C.E., Verheij, C., Willemsen, R., van der Helm, R., Oerlemans, F., Vermey, M., Bygrave, A., Hoogeveen, A., Oostra, B.A., Reyniers, E., Boule, K.D., D'Hooge, R., Cras, P., van Velzen, D., Nagels, G., Martin, J.-J., Deyn, P.P.D., Darby, J.K., Willems, P.J., 1994. Fmr1 knockout mice: a model to study fragile X mental retardation. Cell 78, 23–33. https://doi.org/10.1016/0092-8674(94)90569-X.

Bland, K.M., Casey, Z.O., Handwerk, C.J., Holley, Z.L., Vidal, G.S., 2017. Inducing Cre-lox recombination in mouse cerebral cortex through in utero electroporation. JoVE 56675. https://doi.org/10.3791/56675.

Bureau, I., Shepherd, G.M.G., Svoboda, K., 2008. Circuit and plasticity defects in the developing somatosensory cortex of Fmr1 Knock-out mice. J. Neurosci. 28, 5178–5188. https://doi.org/10.1523/JNEUROSCI.1076-08.2008.

Christie, S.B., Akins, M.R., Schwob, J.E., Fallon, J.R., 2009. The FXG: a presynaptic fragile X granule expressed in a subset of developing brain circuits. J. Neurosci. 29, 1514–1524. https://doi.org/10.1523/JNEUROSCI.3937-08.2009.

Colodner, K.J., Montana, R.A., Anthony, D.C., Folkerth, R.D., De Girolami, U., Feany, M. B., 2005. Proliferative potential of human astrocytes. J. Neuropathol. Exp. Neurol. 64, 163–169. https://doi.org/10.1093/jnen/64.2.163.

Comery, T.A., Harris, J.B., Willems, P.J., Oostra, B.A., Irwin, S.A., Weiler, I.J., Greenough, W.T., 1997. Abnormal dendritic spines in fragile X knockout mice: maturation and pruning deficits. Proc. Natl. Acad. Sci. U. S. A. 94, 5401–5404. https://doi.org/10.1073/pnas.94.10.5401.

Contractor, A., Klyachko, V.A., Portera-Cailliau, C., 2015. Altered neuronal and circuit excitability in fragile X syndrome. Neuron 87, 699–715. https://doi.org/10.1016/j.neuron.2015.06.017.

Cruz-Martín, A., Crespo, M., Portera-Cailliau, C., 2010. Delayed stabilization of dendritic spines in fragile X mice. J. Neurosci. 30, 7793–7803. https://doi.org/10.1523/JNEUROSCI.0577-10.2010.

Davis, J.K., Broadie, K., 2017. Multifarious functions of the fragile X mental retardation protein. Trends Genet. 33, 703–714. https://doi.org/10.1016/j.tig.2017.07.008.

de Vries, B.B., Wiegers, A.M., Smits, A.P., Mohkamsing, S., Duivenvoorden, H.J., Fryns, J. P., Curfs, L.M., Halley, D.J., Oostra, B.A., van den Ouweland, A.M., Niermeijer, M.F., 1996. Mental status of females with an FMR1 gene full mutation. Am. J. Hum. Genet. 58, 1025–1032.

Deng, P.-Y., Rotman, Z., Blundon, J.A., Cho, Y., Cui, J., Cavalli, V., Zakharenko, S.S., Klyachko, V.A., 2013. FMRP regulates neurotransmitter release and synaptic information transmission by modulating action potential duration via BK channels. Neuron 77, 696–711. https://doi.org/10.1016/j.neuron.2012.12.018.

Dölen, G., Osterweil, E., Shankaranarayana Rao, B.S., Smith, G.B., Auerbach, B.D., Chattarji, S., Bear, M.F., 2007. Correction of fragile X syndrome in mice. Neuron 56, 955–962. https://doi.org/10.1016/j.neuron.2007.12.001.

Feng, Y., Gutekunst, C.-A., Eberhart, D.E., Yi, H., Warren, S.T., Hersch, S.M., 1997. Fragile X mental retardation protein: nucleocytoplasmic shuttling and association with somatodendritic ribosomes. J. Neurosci. 17, 1539–1547. https://doi.org/10.1523/JNEUROSCI.17-05-01539.1997.

Feng, G., Mellor, R.H., Bernstein, M., Keller-Peck, C., Nguyen, Q.T., Wallace, M., Nerbonne, J.M., Lichtman, J.W., Sanes, J.R., 2000. Imaging neuronal subsets in transgenic mice expressing multiple spectral variants of GFP. Neuron 28, 41–51. https://doi.org/10.1016/S0896-6273(00)00084-2.

Galvez, R., Greenough, W.T., 2005. Sequence of abnormal dendritic spine development in primary somatosensory cortex of a mouse model of the fragile X mental retardation syndrome. Am. J. Med. Genet. A 135, 155–160. https://doi.org/10.1002/ajmg.a.30709.

Hagerman, R.J., Jackson, C., Amiri, K., O'Connor, R., Sobesky, W., Silverman, A.C., 1992. Girls with fragile X syndrome: physical and neurocognitive status and outcome. Pediatrics 89, 395–400.

Hagerman, R.J., Berry-Kravis, E., Hazlett, H.C., Bailey, D.B., Moine, H., Kooy, R.F., Tassone, F., Gantois, I., Sonenberg, N., Mandel, J.L., Hagerman, P.J., 2017. Fragile X syndrome. Nat. Rev. Dis. Prim. 3, 1–19. https://doi.org/10.1038/nrdp.2017.65.

Hanson, J.E., Madison, D.V., 2007. Presynaptic Fmr1 genotype influences the degree of synaptic connectivity in a mosaic mouse model of fragile X syndrome. J. Neurosci. 27, 4014–4018. https://doi.org/10.1523/JNEUROSCI.4717-06.2007.

Harris, K.M., Jensen, F.E., Tsao, B., 1992. Three-dimensional structure of dendritic spines and synapses in rat hippocampus (CA1) at postnatal day 15 and adult ages: implications for the maturation of synaptic physiology and long-term potentiation. J. Neurosci. 12, 2685–2705.

Hayashi, M.L., Rao, B.S.S., Seo, J.-S., Choi, H.-S., Dolan, B.M., Choi, S.-Y., Chattarji, S., Tonegawa, S., 2007. Inhibition of p21-activated kinase rescues symptoms of fragile X syndrome in mice. PNAS 104, 11489–11494. https://doi.org/10.1073/pnas.0705003104.

He, C.X., Portera-Cailliau, C., 2013. The trouble with spines in fragile X syndrome: density, maturity and plasticity. Neuroscience 251, 120–128. https://doi.org/10.1016/j.neuroscience.2012.03.049.

Higashimori, H., Schin, C.S., Chiang, M.S.R., Morel, L., Shoneye, T.A., Nelson, D.L., Yang, Y., 2016. Selective deletion of Astroglial FMRP dysregulates glutamate transporter GLT1 and contributes to fragile X syndrome phenotypes in vivo. J. Neurosci. 36, 7079–7094. https://doi.org/10.1523/JNEUROSCI.1069-16.2016.

Hodges, J.L., Yu, X., Gilmore, A., Bennett, H., Tjia, M., Perna, J.F., Chen, C.-C., Li, X., Lu, J., Zuo, Y., 2017. Astrocytic contributions to synaptic and learning abnormalities in a mouse model of fragile X syndrome. Biol. Psychiatry 82, 139–149. https://doi.org/10.1016/j.biopsych.2016.08.036.

Irwin, S.A., Patel, B., Idupulapati, M., Harris, J.B., Crisostomo, R.A., Larsen, B.P., Kooy, F., Willems, P.J., Cras, P., Kozlowski, P.B., Swain, R.A., Weiler, I.J., Greenough, W.T., 2001. Abnormal dendritic spine characteristics in the temporal and visual cortices of patients with fragile-X syndrome: a quantitative examination. Am. J. Med. Genet. 98, 161–167. https://doi.org/10.1002/1096-8628(20010115)98:2<161::aid-ajmg1025>3.0.co;2-b.

Kaibara, T., Leung, L.S., 1993. Basal versus apical dendritic long-term potentiation of commissural afferents to hippocampal CA1: a current-source density study. J. Neurosci. 13, 2391–2404. https://doi.org/10.1523/JNEUROSCI.13-06-02391.1993.

Kunz, G., Kirsche, W., Wenzel, J., Winkelmann, E., Neumann, H., 1972. Quantitative untersuchungen über die dendritenspines an pyramidenneuronen des sensorischen cortex der ratte [quantitative studies on the dendrite spines of pyramidal neurons in the rat sensory cortex]. Z Mikrosk Anat Forsch 85, 397–416.

Lein, E.S., Hawrylycz, M.J., Ao, N., Ayres, M., Bensinger, A., Bernard, A., Boe, A.F., Boguski, M.S., Brockway, K.S., Byrnes, E.J., Chen, Lin, Chen, Li, Chen, T.-M., Chi Chin, M., Chong, J., Crook, B.E., Czaplinska, A., Dang, C.N., Datta, S., Dee, N.R., Desaki, A.L., Desta, T., Diep, E., Dolbeare, T.A., Donelan, M.J., Dong, H.-W., Dougherty, J.G., Duncan, B.J., Ebbert, A.J., Eichele, G., Estin, L.K., Faber, C., Facer, B.A., Fields, R., Fischer, S.R., Fliss, T.P., Frensley, C., Gates, S.N., Glattfelder, K.J., Halverson, K.R., Hart, M.R., Hohmann, J.G., Howell, M.P., Jeung, D.P., Johnson, R.A., Karr, P.T., Kawal, R., Kidney, J.M., Knapik, R.H., Kuan, C.L., Lake, J.H., Laramee, A.R., Larsen, K.D., Lau, C., Lemon, T.A., Liang, A.J., Liu, Y., Luong, L.T., Michaels, J., Morgan, J.J., Morgan, R.J., Mortrud, M.T., Mosqueda, N.F., Ng, L.L., Ng, R., Orta, G.J., Overly, C.C., Pak, T.H., Parry, S.E., Pathak, S.D., Pearson, O.C., Puchalski, R.B., Riley, Z.L., Rockett, H.R., Rowland, S.A., Royall, J.J., Ruiz, M.J., Sarno, N.R., Schaffnit, K., Shapovalova, N.V., Sivisay, T., Slaughterbeck, C.R., Smith, S.C., Smith, K.A., Smith, B.I., Sodt, A.J., Stewart, N.N., Stumpf, K.-R., Sunkin, S.M., Sutram, M., Tam, A., Teemer, C.D., Thaller, C., Thompson, C.L., Varnam, L.R., Visel, A., Whitlock, R.M., Wohnoutka, P.E., Wolkey, C.K., Wong, V.Y., Wood, M., Yaylaoglu, M.B., Young, R.C., Youngstrom, B. L., Feng Yuan, X., Zhang, B., Zwingman, T.A., Jones, A.R., 2007. Genome-wide atlas of gene expression in the adult mouse brain. Nature 445, 168–176. https://doi.org/10.1038/nature05453.

Levenga, J., de Vrij, F.M.S., Buijsen, R.A.M., Li, T., Nieuwenhuizen, I.M., Pop, A., Oostra, B.A., Willemsen, R., 2011. Subregion-specific dendritic spine abnormalities in the hippocampus of Fmr1 KO mice. Neurobiol. Learn. Mem. 95, 467–472. https://doi.org/10.1016/j.nlm.2011.02.009.

Liu, Z.-H., Chuang, D.-M., Smith, C.B., 2011. Lithium ameliorates phenotypic deficits in a mouse model of fragile X syndrome. Int. J. Neuropsychopharmacol. 14, 618–630. https://doi.org/10.1017/S1461145710000520.

Loesch, D.Z., Huggins, R.M., Hagerman, R.J., 2004. Phenotypic variation and FMRP levels in fragile X. Ment. Retard. Dev. Disabil. Res. Rev. 10, 31–41. https://doi.org/10.1002/mrdd.20006.

Martínez, R., Bonilla-Henao, V., Jiménez, A., Lucas, M., Vega, C., Ramos, I., Sobrino, F., Pintado, E., 2005. Skewed X inactivation of the normal allele in fully mutated female carriers determines the levels of FMRP in blood and the fragile X phenotype. Mol. Diagn. 9, 157–162. https://doi.org/10.1007/BF03260084.

McKinney, B.C., Grossman, A.W., Elisseou, N.M., Greenough, W.T., 2005. Dendritic spine abnormalities in the occipital cortex of C57BL/6 Fmr1 knockout mice. Am. J. Med. Genet. B Neuropsychiatr. Genet. 136B, 98–102. https://doi.org/10.1002/ajmg.b.30183.

Meredith, R.M., Holmgren, C.D., Weidum, M., Burnashev, N., Mansvelder, H.D., 2007. Increased threshold for spike-timing-dependent plasticity is caused by unreliable calcium signaling in mice lacking fragile X gene FMR1. Neuron 54, 627–638. https://doi.org/10.1016/j.neuron.2007.04.028.

Michalski, A., Patzwaldt, R., Schulz, E., Schonheit, B., 1976. Quantitative Untersuchungen an primitiven Pyramidenzellen in der vorderen cingulären Rinde der Ratte [quantitative study of primitive pyramidal cells in rat anterior cingular cortex]. J. Hirnforsch. 17, 143–153.

Muhammad, A., Carroll, C., Kolb, B., 2012. Stress during development alters dendritic morphology in the nucleus accumbens and prefrontal cortex. Neuroscience 216, 103–109. https://doi.org/10.1016/j.neuroscience.2012.04.041.

Mychasiuk, R., Muhammad, A., Gibb, R., Kolb, B., 2013. Long-term alterations to dendritic morphology and spine density associated with prenatal exposure to nicotine. Brain Res. 1499, 53–60. https://doi.org/10.1016/j.brainres.2012.12.021.

Patel, A.B., Hays, S.A., Bureau, I., Huber, K.M., Gibson, J.R., 2013. A target cell-specific role for presynaptic Fmr1 in regulating glutamate release onto neocortical fast-spiking inhibitory neurons. J. Neurosci. 33, 2593–2604. https://doi.org/10.1523/JNEUROSCI.2447-12.2013.

Patel, A.B., Loerwald, K.W., Huber, K.M., Gibson, J.R., 2014. Postsynaptic FMRP promotes the pruning of cell-to-cell connections among pyramidal neurons in the L5A neocortical network. J. Neurosci. 34, 3413–3418. https://doi.org/10.1523/JNEUROSCI.2921-13.2014.

Paxinos, G., Franklin, K.B.J., 2004. The mouse brain in stereotaxic coordinates, Compact, 2nd ed. Elsevier Academic Press, Amsterdam; Boston.

Petreanu, L., Mao, T., Sternson, S.M., Svoboda, K., 2009. The subcellular organization of neocortical excitatory connections. Nature 457, 1142–1145. https://doi.org/10.1038/nature07709.

Pfeiffer, B.E., Huber, K.M., 2007. Fragile X mental retardation protein induces synapse loss through acute postsynaptic translational regulation. J. Neurosci. 27, 3120–3130. https://doi.org/10.1523/JNEUROSCI.0054-07.2007.

Pfeiffer, B.E., Zang, T., Wilkerson, J.R., Taniguchi, M., Maksimova, M.A., Smith, L.N., Cowan, C.W., Huber, K.M., 2010. Fragile X mental retardation protein is required for synapse elimination by the activity-dependent transcription factor MEF2. Neuron 66, 191–197. https://doi.org/10.1016/j.neuron.2010.03.017.

Rah, J.-C., Bas, E., Colonell, J., Mishchenko, Y., Karsh, B., Fetter, R.D., Myers, E.W., Chklovskii, D.B., Svoboda, K., Harris, T.D., Isaac, J.T.R., 2013. Thalamocortical input onto layer 5 pyramidal neurons measured using quantitative large-scale array tomography. Front. Neural Circuits 7. https://doi.org/10.3389/fncir.2013.00177.

Rais, M., Binder, D.K., Razak, K.A., Ethell, I.M., 2018. Sensory Processing Phenotypes in Fragile X Syndrome. ASN Neuro. https://doi.org/10.1177/1759091418801092.

Reiss, A.L., Freund, L.S., Baumgardner, T.L., Abrams, M.T., Denckla, M.B., 1995. Contribution of the FMR1 gene mutation to human intellectual dysfunction. Nat. Genet. 11, 331–334. https://doi.org/10.1038/ng1195-331.

Rifé, M., Nadal, A., Milà, M., Willemsen, R., 2004. Immunohistochemical FMRP studies in a full mutated female fetus. Am. J. Med. Genet. A 124A, 129–132. https://doi.org/10.1002/ajmg.a.20342.

Rodriguez, A., Ehlenberger, D.B., Hof, P.R., Wearne, S.L., 2006. Rayburst sampling, an algorithm for automated three-dimensional shape analysis from laser scanning microscopy images. Nat. Protoc. 1, 2152–2161. https://doi.org/10.1038/nprot.2006.313.

Rodriguez, A., Ehlenberger, D.B., Dickstein, D.L., Hof, P.R., Wearne, S.L., 2008. Automated three-dimensional detection and shape classification of dendritic spines from fluorescence microscopy images. PLoS One 3, e1997. https://doi.org/10.1371/journal.pone.0001997.

Rueden, C.T., Schindelin, J., Hiner, M.C., DeZonia, B.E., Walter, A.E., Arena, E.T., Eliceiri, K.W., 2017. ImageJ2: ImageJ for the next generation of scientific image data. BMC Bioinfo. 18, 529. https://doi.org/10.1186/s12859-017-1934-z.

Ruszczycki, B., Szepesi, Z., Wilczynski, G.M., Bijata, M., Kalita, K., Kaczmarek, L., Wlodarczyk, J., 2012. Sampling issues in quantitative analysis of dendritic spines morphology. BMC Bioinfo. 13, 213. https://doi.org/10.1186/1471-2105-13-213.

Schindelin, J., Arganda-Carreras, I., Frise, E., Kaynig, V., Longair, M., Pietzsch, T., Preibisch, S., Rueden, C., Saalfeld, S., Schmid, B., Tinevez, J.-Y., White, D.J., Hartenstein, V., Eliceiri, K., Tomancak, P., Cardona, A., 2012. Fiji: an open-source platform for biological-image analysis. Nat. Methods 9, 676–682. https://doi.org/10.1038/nmeth.2019.

Schönheit, B., Schulz, E., 1976. Quantitative Untersuchungen über die Dendriten-spines an den Lamina V-Pyramidenzellen im Bereich der vorderen cingulären Rinde der Ratte [quantitative studies on the dendritic spine distribution on the lamina-5 pyramidal cells in the anterior gyrus cinguli of the rat]. J. Hirnforsch. 17, 171–187.

Sherman, S.L., Jacobs, P.A., Morton, N.E., Froster-Iskenius, U., Howard-Peebles, P.N., Nielsen, K.B., Partington, M.W., Sutherland, G.R., Turner, G., Watson, M., 1985. Further segregation analysis of the fragile X syndrome with special reference to transmitting males. Hum. Genet. 69, 289–299. https://doi.org/10.1007/BF00291644.

Simhal, A.K., Zuo, Y., Perez, M.M., Madison, D.V., Sapiro, G., Micheva, K.D., 2019. Multifaceted changes in synaptic composition and astrocytic involvement in a mouse model of fragile X syndrome. Sci. Rep. 9, 1–16. https://doi.org/10.1038/s41598-019-50240-x.

Steele, J.W., Brautigam, H., Short, J.A., Sowa, A., Shi, M., Yadav, A., Weaver, C.M., Westaway, D., Fraser, P.E., St George-Hyslop, P.H., Gandy, S., Hof, P.R., Dickstein, D.L., 2014. Early fear memory defects are associated with altered synaptic plasticity and molecular architecture in the TgCRND8 Alzheimer's disease mouse model. J. Comp. Neurol. 522, 2319–2335. https://doi.org/10.1002/cne.23536.

Sun, Y.J., Baumer, A., 1999. Nonrandom X inactivation and selection of fragile X full mutation in fetal fibroblasts. Am. J. Med. Genet. 86, 162–164. https://doi.org/10.1002/(SICI)1096-8628(19990910)86:2<162::AID-AJMG14>3.0.CO;2-D.

Turner, G., Brookwell, R., Daniel, A., Selikowitz, M., Zilibowitz, M., 1980. Heterozygous expression of X-linked mental retardation and X-chromosome marker Fra(X)(Q27). N. Engl. J. Med. 303, 662–664. https://doi.org/10.1056/NEJM198009183031202.

Uchida, I.A., Freeman, V.C., Jamro, H., Partington, M.W., Soltan, H.C., 1983. Additional evidence for fragile X activity in heterozygous carriers. Am. J. Hum. Genet. 35, 861–868.

Wang, X., Soloway, P.D., Clark, A.G., 2010. Paternally biased X inactivation in mouse neonatal brain. Genome Biol. 11, R79. https://doi.org/10.1186/gb-2010-11-7-r79.

Wang, G.X., Smith, S.J., Mourrain, P., 2014. Fmr1 KO and Fenobam treatment differentially impact distinct synapse populations of mouse neocortex. Neuron 84, 1273–1286. https://doi.org/10.1016/j.neuron.2014.11.016.

Wang, G.X., Smith, S.J., Mourrain, P., 2016. Sub-synaptic, multiplexed analysis of proteins reveals fragile X related protein 2 is mislocalized in Fmr1 KO synapses. Elife 5. https://doi.org/10.7554/eLife.20560.

Wang, X., Zorio, D.A.R., Schecterson, L., Lu, Y., Wang, Y., 2018. Postsynaptic FMRP regulates synaptogenesis in vivo in the developing cochlear nucleus. J. Neurosci. 38, 6445–6460. https://doi.org/10.1523/JNEUROSCI.0665-18.2018.

Wijetunge, L.S., Angibaud, J., Frick, A., Kind, P.C., Nägerl, U.V., 2014. Stimulated emission depletion (STED) microscopy reveals nanoscale defects in the developmental trajectory of dendritic spine morphogenesis in a mouse model of fragile X syndrome. J. Neurosci. 34, 6405–6412. https://doi.org/10.1523/JNEUROSCI.5302-13.2014.

Zang, T., Maksimova, M.A., Cowan, C.W., Bassel-Duby, R., Olson, E.N., Huber, K.M., 2013. Postsynaptic FMRP bidirectionally regulates excitatory synapses as a function of developmental age and MEF2 activity. Mol. Cell. Neurosci. RNA Splic. Reg. Neurodegen. 56, 39–49. https://doi.org/10.1016/j.mcn.2013.03.002.